applied sciences

MDPI

Article

Settlement Foundations by Exploring the Collapse of Unsaturated Soils

Marieh Fatahizadeh * and Hossein Nowamooz

Le laboratoire des Sciences de L'ingénieur, de L'informatique et de L'imagerie (UMR7357), L'institut National des Sciences Appliquées de Strasbourg (INSA), Université de Strasbourg, F-67081 Strasbourg, France; hossein.nowamooz@insa-strasbourg.fr

* Correspondence: marieh.fatahizadeh@insa-strasbourg.fr

Abstract: Increasing extreme weather events and climate change can significantly affect soil moisture regimes, particularly soil suction, leading to additional challenges associated with unsaturated soils, including the collapse phenomenon. The collapsibility of soils poses significant engineering and geotechnical risks globally, necessitating urgent attention from engineers. This work establishes a numerical model of a shallow foundation subjected to rainfall and load using COMSOL Multiphysics. A hydromechanical model (H-M) is introduced which incorporates The Richards' module and the Extended Basic Barcelona Model (EBBM) as a constitutive model to predict settlements in shallow foundations influenced by climate change and intense rainfall. The validation of the model is conducted through experimental tests, ensuring its accuracy. Additionally, in the practical application, the hydromechanical model is applied to anticipate the effect of infiltration on settlements of shallow foundations. The simulation results show that infiltration leads to an increase in the pressure head above the water table, decreasing soil suction, which induces additional settlement due to wetting-induced collapse. The maximum settlement happened at the corners of the footing due to increased exposure to infiltration and a greater reduction in suction. The collapse potential calculated from the numerical simulation was found to be consistent with the predictions established via analytical models, validating the accuracy of the numerical approach.

Keywords: collapsibility of soils; unsaturated soils; shallow foundation; rainfall

Citation: Fatahizadeh, M.; Nowamooz, H. Settlement Foundations by Exploring the Collapse of Unsaturated Soils. *Appl. Sci.* **2024**, *14*, 7688. https://doi.org/10.3390/app14177688

Academic Editors: Mien Jao and Paul Bernazzani

Received: 13 July 2024
Revised: 16 August 2024
Accepted: 22 August 2024
Published: 30 August 2024

1. Introduction

The collapsibility of soils can contribute to many serious engineering and geotechnical risks all over the world, where these soils are formed naturally or by human activity and are considered to present critical challenges to engineers [1]. However, the rapid increase in the world population resulted in the extension of cities and the construction of new earthwork infrastructure, and the concept of sustainable construction has made it almost inevitable to develop marginal land that may include problematic soil such as collapsible soils. Therefore, it seems necessary to study and understand the mechanisms of these phenomena.

Soil collapse refers to a mechanism by which the total volume of a soil structure, characterized by a metastable open structure, suddenly reduces as a result of loading and/or wetting conditions [2–6]. This volumetric collapse deformation behaviour is often associated with (1) unsaturated conditions, (2) certain physical characteristics such as an open soil structure, large void ratio, and low interparticle bond strength, (3) a relatively high stress level, (4) and a decrease in suction (introduction of additional water), which is recognized as the main triggering factor for collapse deformation [6–9]. The extra water can originate from natural sources, such as rainfall and a rising ground water table, or from human activities, like leaks from canals or water/sewer lines and over-irrigation [2]. Wetting-induced collapse can undermine numerous small structures with shallow foundations and drainage systems. Since the early investigation into collapse phenomena, numerous laboratory and modeling investigations

have been carried out with the aim of enhancing our comprehension of this significant issue. These have tried to develop a laboratory method for determining the wetting-induced collapse of soil [10–14].

Analytical methods including statistical regression-based empirical equations were developed to predict the collapse potential of soil [3,15–20]. Table 1 outlines the various collected models for predicting soil collapse potential.

Table 1. Equations predicting the collapse potential of the soil.

Basma and Tuncer (1992) [3]
$CP = 48.496 + 0.102\ C_u - 0.457\ w_i - 3.533\ \gamma_d + 2.80 \ln(p)$
$CP = 47.506 - 0.072\ (S - C) - 0.439\ w_i - 3.123\ \gamma_d + 2.851 \ln(p)$
Lim and Miller (2004) [15]
$I_c = 9.805 + 0.102\ C_u - 0.261\ w_i - 0.424\ \gamma_d + 0.0580\ PI + 0.0697\ C$
Ayadat and Hanna (2008) [18]
$\varepsilon_w = a(\gamma_d - 15.27) + bw_i + 17$
$a = (-0.036\ C_u) - 1.379$
$b = 0.0006\ {C_u}^2 - 0.089\ C_u + 1.3$
$c = 0.55\ C_u + 38$
Zorlu and Kasapoglu (2009) [17]
$I_c = 0.9081\left[\left(1.3891\ e^{0.0116\ (f_i)}\right) \times (2.3136 \ln(e_0) + 4.3635)\right]^{0.5522}$
Rabbi et al. (2015) [16]
$CP = 3.501 \times (1 - R_d)^{0.687} \times \left(1 - \frac{S_r}{100}\right)^{2.121} \times \left[C^{0.528} \times ln\left\{\frac{p^{1.331}}{p_a}\right\} + 5.719\right]$
Ashour et al. (2020) [19]
$CP = -17.373 + 1.355 \ln(p) + 16.156 e_0 + 21.366\ e^{-5.5 S_r} + 0.00088\ Cu^2$
Alassal et al. (2023) [20]
$CP = 0.206\ p + 0.0016\ (u_a - u_w)_i - 0.0007(p)^2 - 2.7 \times (10)^{-8} \times (u_a - u_w)^2 + X$
($X = -15.15$ for $Dr \approx 35\%$, $w_i = 5\%$, fines content = 40%).

CP: the collapse potential (%); I_c: the collapse index; C_u: the coefficient of uniformity of the soil; *p*: the soaking pressure (kPa); w_i: the initial water content (%); γ_d: the compaction dry unit weight (kN/m3); *C*: the clay-size fraction (%); *S*: the sand-size fraction (%); *Sr*: the degree of saturation (%). *PI*: the plasticity index (%); p_a: the atmospheric pressure (kPa); e_0: the initial void ratio (−); f_i: the fines content (%); *RD*: the dry density ratio (−); $(u_a - u_w)_i$: the matric suction before wetting (kPa); *Dr*: the relative density (%).

Climate change and the increase in the frequency of extreme weather can cause significant changes in the soil moisture regime (soil suction), inducing further problems associated with unsaturated soils including collapse phenomena. The most significant changes are the observed precipitation pattern and the duration of droughts. Prediction models show an increase in the number of 1- to 5-day precipitation extremes for central Europe, attributed to climate change [21]. Bicalho et al. (2014) [22] recorded that the result of a 30 min period of rainfall can considerably influence soil suction changes at the onset of the wet period, especially after experiencing a prolonged dry period. Research by Ng et al. (2003) [23] illustrated that high initial suction, due to a dry season, followed by a rapid increase in water content (and a corresponding reduction in suction) during subsequent wetting, can lead to horizontal stresses and surface soil collapse, especially in the first 1–2 days after the beginning of rainfall. Au (1998) [24] already mentioned that in Hong Kong, landslides are primarily triggered by rainfall. However, laboratory methods have limitations in replicating real-world conditions, and conducting in situ collapse measurements with actual meteorological conditions proves to be challenging.

Constitutive models have been established recently to explain the behavior of unsaturated soils and quantify their collapse. The Barcelona Basic Model (BBM), an unsaturated elasto-plastic critical state model, was developed by Alonso et al. [25]. This mathematical formulation was introduced to simulate the volumetric collapse behavior of unsaturated soils during wetting. Since then, several constitutive models were developed with the aim of enhancing the prediction of unsaturated soils' volumetric behaviour [26–35]. It was confirmed that the BBM elastoplastic model adequately predicts volume change under precipitation [36–40].

In recent years, efforts have been made to develop hydromechanical frameworks that can accurately simulate the wetting-induced soil deformations under various foundation types and different wetting conditions. Xu (2018) [40] presented a hydromechanical model that incorporates stress equilibrium equations and water mass balance, including the BBM and the Soil Water Retention Curve (SWRC), to explain the settlement caused by an elevated groundwater level in loess soils. Achieving favorable consistency between in situ results and numerical simulations, the hydromechanical model is suggested to be efficiently applicable to other loess soils, provided knowledge of SWRC. Investigations reported by Wang et al. (2013) [41] demonstrated that hydromechanical frameworks utilizing the Barcelona Expansive Model (BExM) [42] effectively describe the swelling pressure and microstructural volume changes occurring as suction decreases in bentonite/sand mixtures. Casini (2012) [43] and Kim et al. (2017) [44] successfully implemented the hydro-mechanical models to predict settlements of shallow foundations due to rainfall infiltrations. Liu et al. (2023) [45] investigated the impact of saturated hydraulic conductivity and the duration of rainfall on collapse using the EBBM model. The study concluded that the simulated results generally align with the field results, verifying the hydro-mechanical model's accuracy. Francisca et al. (2024) [46] presented a hydro-mechanical model to analyze strip foundation behavior on loess soil. The calibration involved experimental data and retrofit analysis from full-scale prototypes, proving that the model's prediction of settlements caused by wetting is accurate.

For a more comprehensive understanding of the impacts of climate change, this study investigates the examination of the collapse potential of shallow foundations and footings situated on unsaturated soil. Utilizing COMSOL Multiphysics [47], we have developed a hydromechanical model coupled with a soil mechanics model capable of replicating settlements in shallow foundations attributed to climate change and intense rainfall. The constitutive laws in the hydromechanical model were calibrated, utilizing experimental data derived thorough a literature review. This calibration process serves to validate the accuracy of our COMSOL model. To illustrate the practical application of our research, we present a specific example highlighting the quantifiable influence of infiltration on the collapse of foundations under specific boundary conditions.

2. Adopted Numerical Framework Using EBBM Theoretical to Predict Collapse

The BBM model, a derivative of the Cam clay model, has been extensively applied in the study of unsaturated soils, especially with significant use in finite element method simulations. It is formulated based on the hardening plasticity framework, which adapts the modified Cam-Clay model (MCCM) to account for unsaturated states. However, the BBM model has limitations in its computer implementation. In response, Pedroso and Farias (2011) [48] proposed a modification aimed at addressing the limitations, enabling the modeling of elastoplastic behavior under hydraulic and mechanical stress cycles, namely, the Extended Basic Barcelona Model (EBBM). It incorporates three new features: (1) incorporating a distinctive smooth yield surface; (2) considering the Lode angle's influence through a cross-section of the yield surface and a smooth failure envelope; and (3) integrating the two-yield surfaces concept. These features were implemented to simplify its implementation and avoid issues associated with yield surface nonconvexity. Several simulations of the hypothetical scenarios outlined by Alonoso et al. [25] are replicated using EBBM, and the results obtained are remarkably comparable to those predicted with the BBM, indicating that the extended version can serve as an effective alternative for the original BBM. The compression deformation during wetting-induced collapse is a complicated aspect of unsaturated soil behavior, where there is a considerable interaction between hydraulic and mechanical issues. Numerical models provide valuable insights for exploring this phenomenon and obtaining a deeper understanding of the various parameters affecting it. The hydromechanical model adopted the finite elements program COMSOL to perform the numerical analyses related to wetting-induced collapse. The H-M model incorporates the EBBM as a constitutive model in plain strain and utilizes the Richards

equation [49] for simulating the wetting process. The signs of the pressures, strains, and stress are considered positive when under compression, following the convention of soil mechanics. Two independent stress factors are incorporated by the EBBM model [25,48]: suction s = ua − uw and net mean stress p = p − ua, where p stands for mean stress, uw stands for pore water pressure, and ua stands for pore air pressure.

2.1. Elastic Deformation

The volumetric elastic strain ($\varepsilon_{e,v}$) can be calculated from the elastic strains induced by both suction ($\varepsilon^{s}_{e,v}$) and pressure ($\varepsilon^{p}_{e,v}$).

$$\varepsilon_{e,v} = \varepsilon^{p}_{e,v} + \varepsilon^{s}_{e,v} \quad (1)$$

The volumetric elastic strain due to pressure can be defined as follows:

$$\varepsilon^{p}_{e,v} = -\frac{dp}{K} \quad (2)$$

where K represents the bulk modulus.

The volumetric elastic strain from suction changes can be expressed as follows:

$$\varepsilon^{s}_{e,v} = -\frac{K_s}{1+e_0}\frac{ds}{(s+p_{atm})} \quad (3)$$

where s is the suction, p_{atm} refers to atmospheric pressure, K_s corresponds to the swelling index for suction changes, and e_0 represents the initial void ratio.

The stress tensor (σ), the shear modulus (G), and the elastic strain (ε_e) have the following relationship:

$$\sigma = dev(\sigma_0) + p\mathbf{I} + 2Gdev(\varepsilon_e) \quad (4)$$

σ_0 denotes the initial or external, $\mathbf{I}$ corresponds to the identity matrix, ε_e signifies the elastic strain tensor, and G represents the shear modulus as follows:

$$G = \frac{(1+e_0)}{K}\, p\, \frac{3-6\upsilon}{2(1+\upsilon)} \quad (5)$$

v is Poisson' ratio.

2.2. Plastic Deformation

A plastic strain matrix can be derived using λp, the plastic multiplier; g, the plastic potential; and q, the deviator stress:

$$\dot{\varepsilon_p} = \lambda_p\left(-\frac{1}{3}\frac{\partial g}{\partial p}I + \frac{\partial g}{\partial q}\frac{3}{2q}dev(\sigma)\right) \quad (6)$$

Based on the associated flow rule, g, the plastic potential is considered identical to the yield function F.

The yield function (F) of EBBM (see Figure 1) is as follows:

$$F = q^2 - M^2(p+p_s)(p_c-p) + {p_{ref}}^2\left(e^{\frac{b(s-s_y)}{p_{ref}}} - e^{\frac{-bs}{p_{ref}}}\right) \quad (7)$$

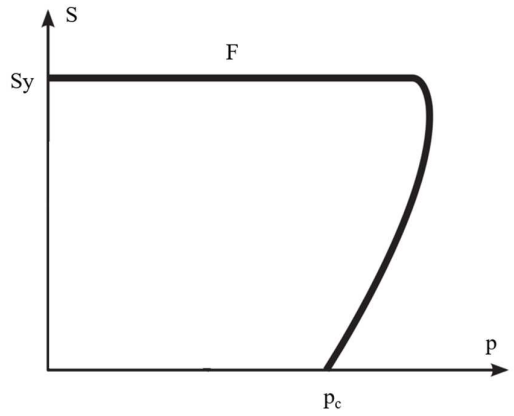

Figure 1. Unique yield surface of the EBBM [48].

Here, M represents the slope of the critical state line, (p_s = k.s), p_s relates to the impact of suction on the soil's cohesiveness, k is a parameter characterizing the increase in cohesion due to suction, p_{ref} indicates the reference pressure, b is described as a smoothing parameter, and s_y is the suction yield value (Figure 1).

p_c represents the preconsolidation pressure corresponding to the current suction value:

$$\frac{p_{cs}}{p_{ref}} = \left(\frac{p_c}{p_{ref}}\right)^{\left[\frac{\lambda(0)-K}{\lambda(S)-K}\right]}; \lambda(s) = \lambda(0)\left[(1-w)\exp\left(\frac{-s}{m}\right)+w\right] \quad (8)$$

p_{cs} is the consolidation pressure in a saturated sate (zero suction), K is the swelling index, $\lambda(s)$ is the slope of the normal compression line corresponding to the current suction (s), and $\lambda(0)$ represents the slope at zero suction. m and w refer to soil stiffness and weighting parameters, respectively.

Equation (8) considers the effect of suction, which is linked to the degree of saturation using SWRC. When the suction decreases in response to infiltration, the yield surface reduces, crossing the LC curve and leading to irreversible volume change, and consequently, the soil undergoes collapse.

The volumetric plastic strains $\varepsilon_{p,v}$ directly influence the change in the consolidation pressure, which governs the hardening characteristics in the stress–strain relationship:

$$\dot{p_c} = -\frac{1+e_0}{\lambda(0)-K} p_c \dot{\varepsilon_{p,v}} \quad (9)$$

However, by increasing the suction, when the suction reaches the yield suction s = s_y, the plastic volumetric strain resulting from yielding on the SI yield surface can be expressed as follows:

$$\dot{p_c} = -\frac{1+e_0}{\lambda_S - K_S}(s_y + p_{atm})\dot{\varepsilon_{p,v}} \quad (10)$$

Appendix A provides a detailed description of the Richards equation. The relative water permeability function has been characterized using the Van Genuchten (1980) [50] and Mualem (1976) models [51] (see Appendix A). SWRC demonstrates a hysteresis effect, reflecting that the relationship between the suction and water content is not unique. During the drying path, increasing suction induces pore water to be displaced by air from the voids. In contrast, during the wetting process, water infiltrates the voids, leading to a reduction in suction [39,52,53]. Since the majority of soil compression occurs as the soil becomes saturated, it is usually more suitable to apply the wetting path of SWRC rather than the drying path when analyzing the soil foundation in the context of rainfall infiltration [54]. To establish the wetting path curve of the investigated soil, the drying path curve was initially fitted using the Johari and Hooshmand Nejad (2018) method [55]. Subsequently,

the wetting path curve was derived using their approach and by applying the parameters recommended in the research of Pham et al. (2005) [56].

3. Validation of the Theoretical Framework

For accurate prediction results and the successful application of the EBBM model in COMSOL, it is necessary to validate the model. To achieve this, an oedometer test was conducted, applying the wetting path on a compacted soil [57]. The soil is characterized as a low-plasticity, poorly graded type, and the proportion of the clay was 17%, while that of the fine sand was greater than 50%. The specific gravity of the soil was 2.69. The Atterberg limits were 25% for the plastic limit and 12% for the liquid limit. The initial void ratio and initial dry density were 0.67 and 1.61 Mg/m^3, respectively.

In the conducted oedometer test, the samples were initially subjected to an increase in vertical stress up to 0.4 MPa under constant water content (suction = 0.2 MPa). Subsequently, wetting occurred under constant vertical stress, and the specific stress path performed for the samples is illustrated in Figure 2. To ensure the accurate replication of the experimental conditions, the bottom border was set in both vertical and horizontal directions, and the vertical boundaries were only constrained horizontally. The same stress path as in the experimental condition was applied. The model's input parameters of EBBM were sourced from the literature [25] (see Table 2). Notably, the smoothing parameter, a new addition for EBBM, was set to b = 100. The comparison between the experimental and predicted results, as depicted in Figure 3, revealed a commendable agreement with only a maximum deviation of approximately 4%. This validates the accuracy of the EBBM model.

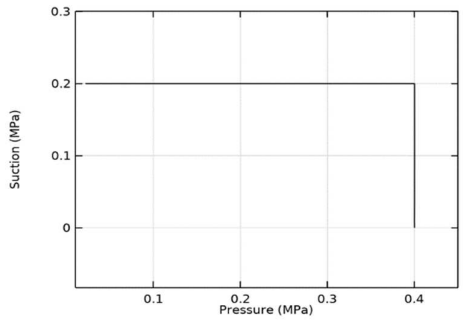

Figure 2. Stress path applied in the oedometer test.

Table 2. EBBM parameters related to the studied soil.

	Description	Value
G	Shear modulus	7 [MPa]
K	Swelling index	0.0077
Ks	Swelling index for variation in suction	0.001
λ(0)	Compression index at zero suction	0.066
λs	Compression index for variation in suction	0.025
P_{ref}	Reference pressure	0.012 [MPa]
P_0^*	Initial preconsolidation pressure	0.02 [MPa]
w	Weight parameter	0.25
m(1/β)	Soil stiffness parameter	0.05 [MPa]
b	Plastic potential parameter	100
Sy0	Initial yield value for suction	0.3 [MPa]
k_s	Tension-to-suction ratio	0.8
M	Slope of critical state line	1.2

Table 3 presents the hydraulic parameters of the studied soil, derived from the estimated wetting curve. The values of Van Genuchten parameters (α, n, θ_s, and θ_r) along the drying path and K_s are derived from the UNSODA (UNsaturated SOil hydraulic DAtabase) database. The data are easily accessible through the UNSODA [58]. Soil reference

2642 corresponds closely to the selected soil in terms of both texture and porosity. Then, the wetting parameters are determined using the methods of Johari and Hooshmand Nejad, 2018 [55] and Pham et al., 2005 [56] (see Figure 4). The parameters, χ_p and χ_f signify the soil matrix's compressibility and the compressibility of water, respectively.

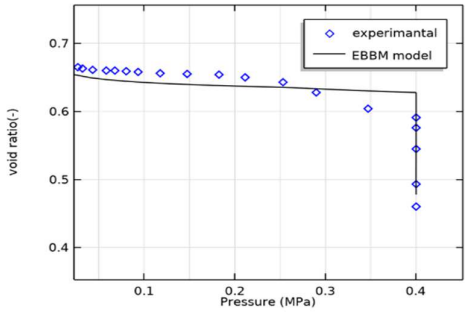

Figure 3. Variation in void ratio with vertical stress.

Table 3. Summary of hydraulic parameters related to the studied soil.

Parameter	Value
Ks	0.75 [m/day]
α	0.44 [1/m]
n	1.103
l	0.5
θ_r	3.59×10^{-23}
θ_s	0.37
χ_f	4×10^{-10} [1/Pa]
χ_p	1×10^{-4} [1/Pa]

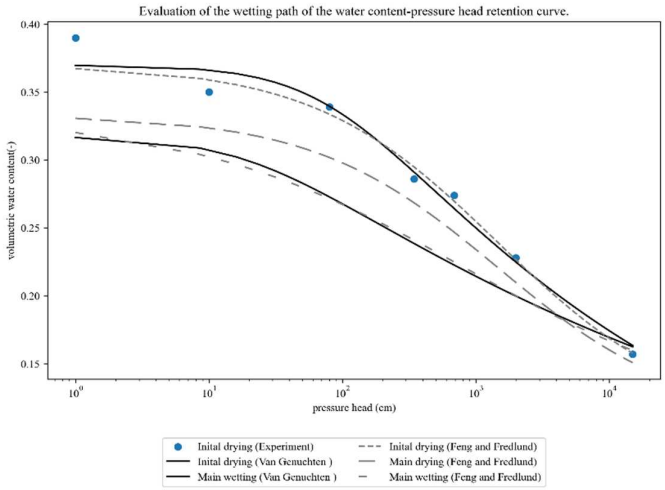

Figure 4. Evaluation of the wetting path of SWRC.

4. Development of a Deterministic Framework Affected by Rainfall Infiltration on the Collapsibility of the Foundation

Infiltration is an extremely complex unsaturated seepage process which can be effectively described by Richards' equation [49,59,60]. Here, the infiltration process was modelled in the hydromechanical framework using Richards' equation and the Van Genuchten retention curve [50].

A 2D model was constructed using Comsol Multiphysics version 6.1. It features a shallow foundation with a length of 1.5 m and a thickness of 0.3 m, which is based on a homogeneous layer of compacted soil (lower Cromer till). The soil is assumed to exhibit elastoplastic behavior and characterized by the EBBM, with parameters determined in the

previous part. Figure 5 exhibits the model's geometry, where the soil domain was defined as having a width of 6 m and a height of 2 m.

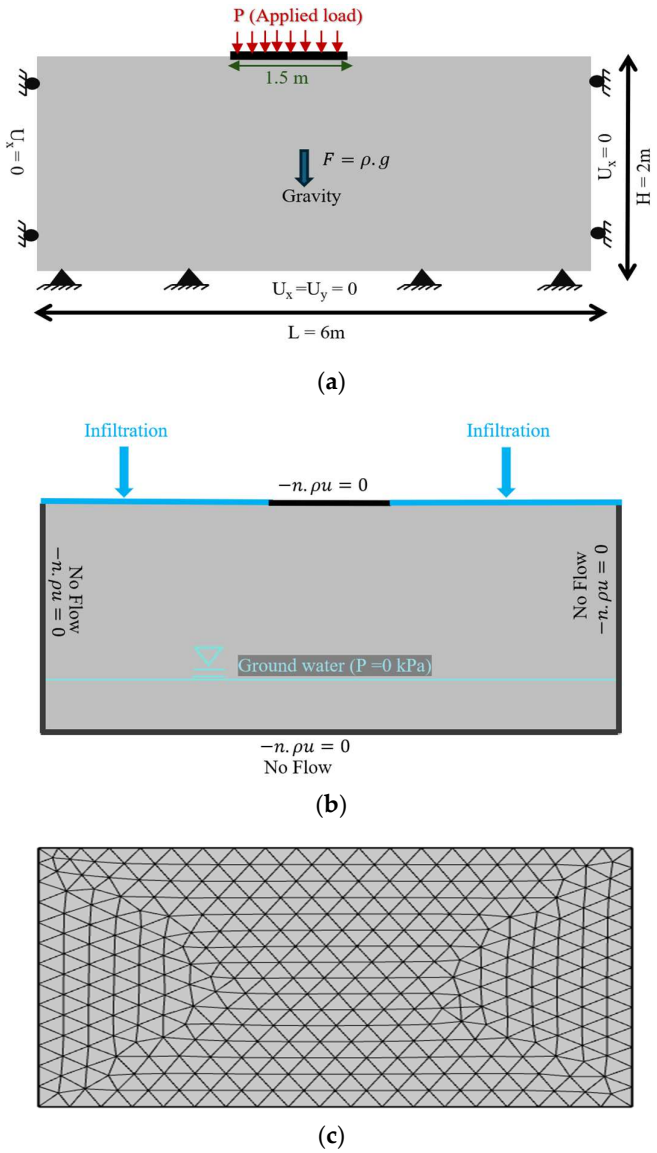

Figure 5. Finite element mesh and geometry. (**a**) Mechanical boundary conditions. (**b**) Mechanical boundary conditions. (**c**) Adopted mesh.

Figure 5a presents the mechanical boundary conditions. Vertical displacements are constrained at the lower base of the soil mass (at a depth of 2 m). Horizontal displacements are also restricted at the vertical boundaries of the soil domain (lateral boundaries). Prior to any mechanical or hydraulic loading, an initial stress state corresponding to the self-weight of the soil is established. Gravity, or weight force, is therefore represented as body force throughout the whole volume of the layer. Initially, the study assumed a stationary condition, introducing the 100 kPa load that was incrementally increased following a linear parametric function to reproduce the construction process.

Figure 5b illustrates the hydraulic boundary conditions. Lateral boundaries allow no mass flux for water, meaning zero mass transfer. Considering the waterproofing inside the building, a zero-mass flux for water is applied at the boundary beneath the building. The water table, located 1.35 m below the surface, defines a pressure of 0 kPa at this depth. The initial conditions of the model are set based on the measured water content and soil suction at different depths, corresponding to the hydrostatic condition. The suction throughout the

soil profile changes linearly from 200 kPa at the surface to 0 kPa at the 1.35 depth. The main boundary condition of the model is the infiltration rate. We considered that precipitation occurs over a 60-day period, considering an infiltration rate of 40 mm/day. These boundary conditions can be applied as an atmospheric time-dependent boundary to the surface of the soil, as shown in Figure 5b. This can be applied using an inlet boundary condition, defining the normal inflow velocity.

Figure 5c shows the adopted mesh. It was applied to the entire domain using a free triangular mesh type, including 1269 triangular elements and 681 mesh vertices. The mesh quality was entirely assessed, with a 0.72 element quality minimum and an element quality average of 0.94, producing a well-structured mesh suitable for precise numerical simulations. The element area ratio is 0.42. The minimum element size is 3.75×10^{-4} m, and the maximum element size is 0.11 m.

In summary, the analysis consists of three phases. Initially, a vertical stress of 100 kPa is applied. Subsequently, infiltration is simulated by applying a boundary condition with a 40 mm/day infiltration rate for 60 days. Positive pressure values ($Hp \geq 0$), derived from the hydraulic model, representing pore pressure, were incorporated into the EBBM to calculate effective stresses. Negative pressure values ($Hp < 0$) expressed as a positive value ($-Hp$) were introduced into the EBBM as suction. The wetting-induced collapses were assessed by assuming that the applied vertical load remained constant. COMSOL Multiphysics 6.1 software incorporates both the EBBM model and the Richards' equation as built-in modules. The coupling in the hydromechanical model is partial: although changes in pore pressure affect soil deformation, the resulting deformation itself has no impact on pore pressure.

4.1. Hydraulic Variation

The settlement's evolution over time was calculated for both the footing and transient flow condition. A 100 kPa load was subjected to the footing. A transient water flow simulation was then performed to model a 60-day rainfall. Figure 6 shows the evolution of the pressure head based on the findings of the numerical models. The pressure head in the soil domain is presented before and after 60 days of rainfall. The pressure head after 60 days of rainfall shows changes above the water table due to the infiltration rate. An increase in the pressure head is observed above the water table. It should be noted that below the foundation, there is a zone in which the pressure does not change due to the waterproofing of the building.

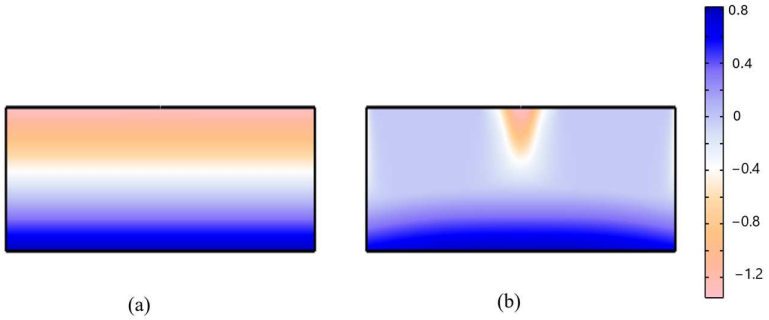

Figure 6. The evolution of the pressure head (m): (**a**) before infiltration and (**b**) after filtration.

Figure 7 highlights the changes in the suction profile resulting from infiltration at different depths and times, both at the center and corners of the foundation. The initial suction was adjusted at 13 kPa at the top and at 0 kPa at a depth of 0.65 m and below, reflecting the natural water content. Figure 7a shows the results of the simulation for the suction profile changes over 60 days at the corner of the footing. After this period, almost all the soil at the corner of the footing becomes nearly saturated (Figure 7b).

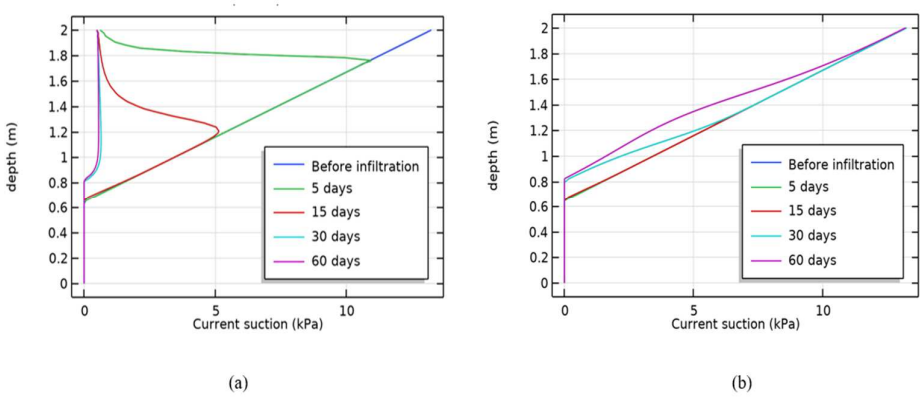

Figure 7. Suction profile changes with depth due to wetting: (**a**) at the corner of the footing and (**b**) at the center of the footing.

4.2. Collapse Settlements

Figure 8 illustrates the variation in λ(s), the compression index, at the current suction within the soil layer. Before the rain, λ(s) is only governed by the initial conditions and is adopted in the numerical model. However, when the infiltration starts, λ(s) is determined from the suction calculated by the hydraulic model. During the infiltration, the λ(s) values change, leading to deformation in the foundation. After 60 days of infiltration, the λ(s) values, except in some parts below the footing, become nearly the same as λ(0) in almost all parts of the soil profile.

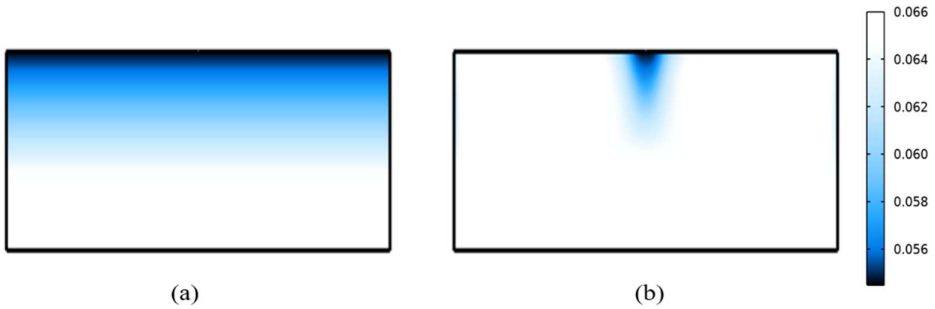

Figure 8. The evolution of the compression index (−): (**a**) before infiltration and (**b**) after infiltration.

The footing pressure versus the settlement after the infiltration is shown in Figure 9. As can be seen, infiltration causes an additional settlement at a constant footing pressure. This additional settlement reproduces the behavior of the unsaturated soil upon wetting, known as wetting-induced collapse, as shown in Figure 9. This indicates that when the soil is gradually wetted, the suction is reduced, resulting in additional settlement until it becomes fully saturated. The apparent pre-consolidation stress and cohesion diminish as a result of the decreased suction, which in turn decreases the soil's yield surface and, eventually, the strength of the soil. This poses a major stability concern, even in soils like sandy soil [61]. This phenomenon is captured by the EBBM model, which takes into account the reduction in suction caused by infiltration and the corresponding decrease in strength.

The vertical displacement of the top layer due to rainfall is presented in Figure 10. It is worth mentioning that the maximum vertical displacement is not centered on the footing but displaced toward the corner. This is because the corner of the footing is exposed to more infiltration and experiences a greater reduction in suction, as depicted in Figure 7. According to the results, the profile of suction at 30 and 60 days nearly remains unchanged. This trend can be attributed to most of the soil collapse occurring within 30 days of infiltration. However, at the center of the footing, the suction profile shows less reduction, which results in a less deformation (see Figure 10). Figure 11 shows the settlement induced by infiltration in the shallow foundation. Initially, the rate of collapse potential is high, but toward the final days, the soil layer experiences minimal settlement,

with insignificant volumetric changes. This is because when the suction approaches zero, the structure experiences insignificant settlement and negligible volumetric changes.

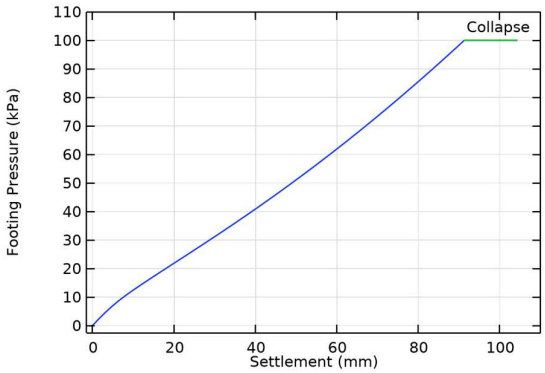

Figure 9. Footing pressure versus settlement.

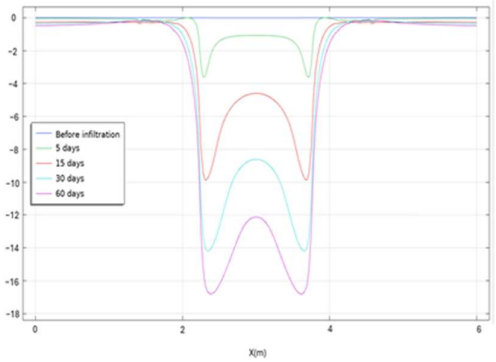

Figure 10. Vertical Displacement of Soil due to Infiltration.

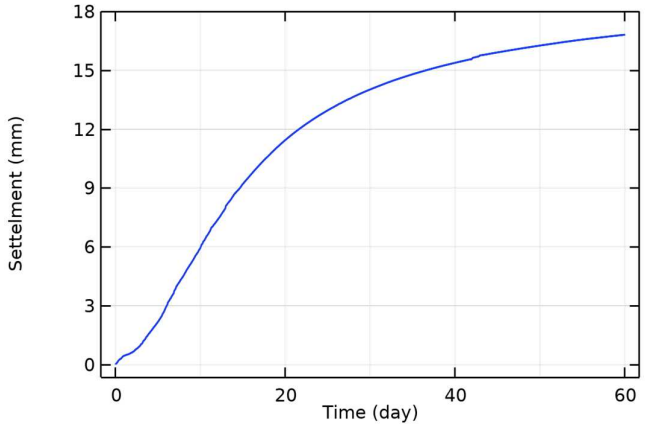

Figure 11. Induced settlement by infiltration in a shallow foundation.

Figure 12 shows the volumetric plastic strain of the soil profile. Generally, during the loading phase (before raining), the peak values of volumetric plastic are concentrated around the footing. However, the collapse of the soil layer induces a considerable expansion of the plastic zone after 60 days of infiltration, with the maximum plastic deformations occurring around the corner of the footing at the surface. Under such conditions, infiltration triggers plastic yielding, resulting in a reduction in the soil volume. This behavior, which contributes to the collapse of the soil, is effectively represented by the EBMM model.

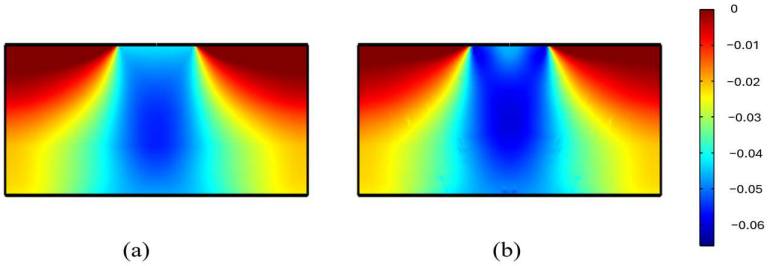

Figure 12. Volumetric plastic strain (−): (**a**) before infiltration and (**b**) after filtration.

To evaluate the collapse potential of this studied soil, the following simple equation can be used:

$$CP = \frac{\Delta H}{H} \times 100 \tag{11}$$

H is the layer's height and ΔH is its maximum vertical settlement. If we assume that the active layer is above the groundwater and that the entire layer is wetted, then H0 = 1.35 m and $\Delta H = 17$ mm. Based on this calculation, the collapse potential is 1.5%.

Given the available information about the soil, two models can be used to predict the collapse potential through analytical modeling: the Basma and Tuncer (1992) model [3] and the Zorlu and Kasapoğlu (2009) model [17]. The collapse potential prediction with the Basma and Tuncer (1992) model [3] is 2.7%, and with the Zorlu and Kasapoğlu (2009) [17] model, it is 2.8%. These predictions are relatively close to the result found in the numerical simulation, which is 1.5%. This comparison shows that the numerical solution respects the field reality and matches the prediction of the analytical solutions.

5. Conclusions

This study shows that the finite element method, in conjunction with an appropriate constitutive model, can be applied to simulate the mechanical and hydraulic properties of unsaturated soil and foundation stability under transient flow conditions. The EBMM constitutive model can successfully represent the mechanical behavior of unsaturated soils, especially in predicting geotechnical issues such as the collapse of the soil. The evolution of settlements was explored for a footing under infiltration during a 60-day rainfall event. The finding shows that 60 days of infiltration caused a significant increase in the pressure head, resulting in a reduction in soil suction above the water table. This reduction in suction results in additional settlement because of the wetting-induced collapse of the soil. The maximum vertical displacement was not observed at the center of footing but shifted towards the corners, where it was exposed to more infiltration and soil suction reduction. The study points out that the rate of collapse potential decreases over time, and negligible settlement is observed as the soil approaches full saturation.

Furthermore, there was good concordance between the predictions made by the analytical models and the numerical simulation results, which validates the reliability of the numerical method adopted in this study. Overall, this study offers invaluable insights into how unsaturated soils behave under infiltration, highlighting the significance of considering the infiltration influences on soil stability and foundation design, particularly in regions prone to heavy rainfall, where a decrease in suction can lead to significant reductions in soil strength and increased settlement.

Author Contributions: Writing—original draft, M.F.; Supervision, H.N. All authors have read and agreed to the published version of the manuscript.

Funding: This research received no external funding.

Institutional Review Board Statement: Not applicable.

Informed Consent Statement: Not applicable.

Data Availability Statement: The original contributions presented in the study are included in the article, further inquiries can be directed to the corresponding author.

Conflicts of Interest: The authors declare no conflict of interest.

Appendix A

Water in porous media, such as soil, is commonly considered to be incompressible, and there is no mass transfer involving soil particles. Since water vapor is excluded from consideration, it is not taken into account. To evaluate the change in water potential over time and space, Richard's equation [49] is used. The general form of this equation is as follows:

$$\rho_w.c_m.\frac{\partial h}{\partial t} + \rho_w \cdot \nabla \cdot [-K.K_r \cdot \nabla h] = Q_m \quad \text{(A1)}$$

where ρ_w is the water density (kg.m^3); h is the hydraulic head (m); C_m denotes the specific moisture capacity (m^{-1}) derived from [50]; κ and κ_r give the hydraulic conductivity of the porous media and the relative hydraulic conductivity, respectively (m.s^{-1}); g (m.s^{-2}) is the acceleration of gravity; and Q_m is the water source exchange (kg.m^{-3}.s^{-2}).

Van Genuchten's (1980) model [50] is employed to calculate relative saturation and suction.

$$S_e = \begin{cases} \frac{1}{\left[1+\left(\alpha \frac{s}{\rho w\ g}\right)^{n}\right]^{m}}, & s > 0 \\ 1, & s \leq 0 \end{cases} \quad \text{(A2)}$$

Here, s stands for suction and α, n, and m ($m = 1 - \frac{1}{n}$) represent van Genuchten parameters. According to the Mualem (1976) models [51] $\left(m = 1 - \frac{1}{n}\right)$, Se is the effective saturation. By knowing the effective saturation and saturated and residual volumetric water content, the current volumetric water content is easily obtained through the following expression: $\theta = \theta_r + S_e(\theta_s - \theta_r)$. θ_s and θ_r are the residual and saturated volumetric water contents, respectively. The degree of saturation (S_r) is also obtained through $S_r = \frac{\theta}{\theta_s}$.

The specific moisture capacity is given by

$$C_m = \begin{cases} \frac{\alpha m}{1-m}(\theta_s - \theta_r)\, S_e^{\frac{1}{m}} \left(1 - S_e^{\frac{1}{m}}\right)^{m}, & s > 0 \\ 1, & s \leq 0 \end{cases} \quad \text{(A3)}$$

The relative water permeability function is defined as [51]

$$k_r = \begin{cases} S_e^{\frac{1}{2}} \left[1 - \left(1 - S_e^{\frac{1}{m}}\right)^{m}\right]^2, & s > 0 \\ 1, & s \leq 0 \end{cases} \quad \text{(A4)}$$

References

1. Mahmood, M.S.; Abrahim, M.J. A Review of Collapsible Soils Behavior and Prediction. *IOP Conf. Ser. Mater. Sci. Eng.* **2021**, *1094*, 012044. [CrossRef]
2. Al-Rawas, A.A. State-of-the-Art-Review of Collapsible Soils. *Sultan Qaboos Univ. J. Sci.* **2000**, *5*, 115–135. [CrossRef]
3. Basma, A.A.; Tuncer, E.R. Evaluation and Control of Collapsible Soils. *J. Geotech. Eng.* **1992**, *118*, 1491–1504. [CrossRef]
4. Opukumo, A.W.; Davie, C.T.; Glendinning, S.; Oborie, E. A Review of the Identification Methods and Types of Collapsible Soils. *J. Eng. Appl. Sci.* **2022**, *69*, 17. [CrossRef]
5. Reznik, Y.M. Influence of Physical Properties on Deformation Characteristics of Collapsible Soils. *Eng. Geol.* **2007**, *92*, 27–37. [CrossRef]
6. Rogers, C. Types and Distribution of Collapsible Soils. In *Genesis and Properties of Collapsible Soils*; Springer: Dordrecht, The Netherlands, 1995; Volume 468, pp. 1–17.
7. Fredlund, D.; Gan, J.K. The Collapse Mechanism of a Soil Subjected to One-Dimensional Loading and Wetting. In *Genesis and Properties of Collapsible Soils*; Springer: Dordrecht, The Netherlands, 1995; Volume 468, pp. 173–198.
8. Houston, S.; Houston, W.N. *Collapsible Soils Engineering*; Geotechnical Special Publication: Reston, VA, USA, 1997.
9. Li, P.; Vanapalli, S.; Li, T. Review of Collapse Triggering Mechanism of Collapsible Soils Due to Wetting. *J. Rock Mech. Geotech. Eng.* **2016**, *8*, 256–274. [CrossRef]

10. Barrera, M.; Romero, E.; Lloret, A.; Gens, A. Collapse Test on Isotropic and Anisotropic Compacted Soils. In *Experimental Evidence and Theoretical Approaches in Unsaturated Soils*, 1st ed.; CRC Press: London, UK, 2000; pp. 14–28.
11. El Howayek, A.; Huang, P.-T.; Bisnett, R.; Santagata, M.C. *Identification and Behavior of Collapsible Soils*; Joint Transportation Research Program; Purdue University: West Lafayette, IN, USA, 2011.
12. Jennings, J.E.B.; Knight, K. A Guide to Construction on or with Materials Exhibiting Additional Settlement Due to "Collapse" of Grain Structure. In Proceedings of the 6th Regional Conference for Africa on Soil Mechanics and Foundation Engineering, Durban, Africa, September 1975; pp. 99–105. Available online: https://pascal-francis.inist.fr/vibad/index.php?action=getRecordDetail&idt=PASCALGEODEBRGM7720382974 (accessed on 21 August 2024).
13. Lawton, E.C.; Fragaszy, R.J.; Hetherington, M.D. Review of Wetting-Induced Collapse in Compacted Soil. *J. Geotech. Eng.* **1992**, *118*, 1376–1394. [CrossRef]
14. Vilar, O.M.; Rodrigues, R.A. Collapse Behavior of Soil in a Brazilian Region Affected by a Rising Water Table. *Can. Geotech. J.* **2011**, *48*, 226–233. [CrossRef]
15. Lim, Y.Y.; Miller, G.A. Wetting-Induced Compression of Compacted Oklahoma Soils. *J. Geotech. Geoenviron. Eng.* **2004**, *130*, 1014–1023. [CrossRef]
16. Rabbi, A.T.M.Z.; Rahman, M.; Cameron, D. Prediction of Collapse Potential for Silty Glacial Sand. Aust. *Geomech. J.* **2014**, *49*, 45–55.
17. Zorlu, K.; Kasapoglu, K. Determination of Geomechanical Properties and Collapse Potential of a Caliche by in Situ and Laboratory Tests. *Environ. Geol.* **2009**, *56*, 1449–1459. [CrossRef]
18. Ayadat, T.; Hanna, A. Effects of Hydraulic Shear Stress and Rate of Erosion on the Magnitude, Degree, and Rate of Collapse. *Geomech. Geoeng.* **2008**, *3*, 59–69. [CrossRef]
19. Ashour, M.; Abbas, A.; Altahrany, A.; Alaaeldin, A. Modelling the Behavior of Inundated Collapsible Soils. *Eng. Rep.* **2020**, *2*, e12156. [CrossRef]
20. Alassal, M.A.; Hassan, A.M.; Elmamlouk, H.H. Collapse Potential Prediction and Characteristics of Unsaturated Sandy Soils. *Geotech. Geol. Eng.* **2023**, *41*, 2759–2774. [CrossRef]
21. Frei, C.; Schöll, R.; Fukutome, S.; Schmidli, J.; Vidale, P.L. Future Change of Precipitation Extremes in Europe: Intercomparison of Scenarios from Regional Climate Models. *J. Geophys. Res. Atmos.* **2006**, *111*, D6. [CrossRef]
22. Bicalho, K.; Cui, Y.; Camporez, L. Study of Climatic Effects on the Soil Suction and Water Content Changes in an Embankment Constructed with Two Clays. *Comun. Geol.* **2014**, *101*, 1405–1407.
23. Ng, C.W.W.; Zhan, L.T.; Bao, C.G.; Fredlund, D.G.; Gong, B.W. Performance of an Unsaturated Expansive Soil Slope Subjected to Artificial Rainfall Infiltration. *Geotechnique* **2003**, *53*, 143–157. [CrossRef]
24. Au, S. Rain-Induced Slope Instability in Hong Kong. *Eng. Geol.* **1998**, *51*, 1–36. [CrossRef]
25. Alonso, E.E.; Gens, A.; Josa, A. A Constitutive Model for Partially Saturated Soils. *Géotechnique* **1990**, *40*, 405–430. [CrossRef]
26. Cui, Y.; Delage, P. Yielding and Plastic Behaviour of an Unsaturated Compacted Silt. *Géotechnique* **1996**, *46*, 291–311. [CrossRef]
27. Georgiadis, K.; Potts, D.M.; Zdravkovic, L. Three-Dimensional Constitutive Model for Partially and Fully Saturated Soils. *Int. J. Geomech.* **2005**, *5*, 244–255. [CrossRef]
28. Kavvadas, M.; Amorosi, A. A Constitutive Model for Structured Soils. *Géotechnique* **2000**, *50*, 263–273. [CrossRef]
29. Romero, E.; Sánchez, M.; Gai, X.; Barrera, M.; Lloret, A. Mechanical Behavior of an Unsaturated Clayey Silt: An Experimental and Constitutive Modelling Study. *Can. Geotech. J.* **2019**, *56*, 1461–1474. [CrossRef]
30. Savvides, A.A.; Papadrakakis, M. A Computational Study on the Uncertainty Quantification of Failure of Clays with a Modified Cam-Clay Yield Criterion. *SN Appl. Sci.* **2021**, *3*, 659. [CrossRef]
31. Sheng, D.; Fredlund, D.G.; Gens, A. A New Modelling Approach for Unsaturated Soils Using Independent Stress Variables. *Can. Geotech. J.* **2008**, *45*, 511–534. [CrossRef]
32. Sheng, D.; Gens, A.; Fredlund, D.G.; Sloan, S.W. Unsaturated Soils: From Constitutive Modelling to Numerical Algorithms. *Comput. Geotech.* **2008**, *35*, 810–824. [CrossRef]
33. Thu, T.M.; Rahardjo, H.; Leong, E.-C. Elastoplastic Model for Unsaturated Soil with Incorporation of the Soil-Water Characteristic Curve. *Can. Geotech. J.* **2007**, *44*, 67–77. [CrossRef]
34. Vaunat, J.; Cante, J.; Ledesma, A.; Gens, A. A Stress Point Algorithm for an Elastoplastic Model in Unsaturated Soils. *Int. J. Plast.* **2000**, *16*, 121–141. [CrossRef]
35. Wheeler, S.; Sivakumar, V. An Elasto-Plastic Critical State Framework for Unsaturated Soil. *Géotechnique* **1995**, *45*, 35–53. [CrossRef]
36. Ali, T.; Showkat, R.; Babu, G.S. Hydro-Mechanical Simulations of Unsaturated Soil Slope. *Indian Geotech. J.* **2021**, *51*, 861–869. [CrossRef]
37. Jamei, M.; Guiras, H.; Olivella, S. Analysis of Slope Movement Initiation Induced by Rainfall Using the Elastoplastic Barcelona Basic Model. *Eur. J. Environ. Civ. Eng.* **2015**, *19*, 1033–1058. [CrossRef]
38. Le, T.M.H.; Gallipoli, D.; Sanchez, M.; Wheeler, S. Rainfall-Induced Differential Settlements of Foundations on Heterogeneous Unsaturated Soils. *Géotechnique* **2013**, *63*, 1346–1355. [CrossRef]
39. Showkat, R.; Babu, G.S. Deterministic and Probabilistic Analysis of the Response of Shallow Footings on Unsaturated Soils Due to Rainfall. *Transp. Geotech.* **2023**, *43*, 101150. [CrossRef]
40. Xu, Y.; Leung, C.; Yu, J.; Chen, W. Numerical Modelling of Hydro-Mechanical Behaviour of Ground Settlement Due to Rising Water Table in Loess. *Nat. Hazards* **2018**, *94*, 241–260. [CrossRef]

41. Wang, Q.; Tang, A.M.; Cui, Y.-J.; Barnichon, J.-D.; Ye, W.-M. Investigation of the Hydro-Mechanical Behaviour of Compacted Bentonite/Sand Mixture Based on the BExM Model. *Comput. Geotech.* **2013**, *54*, 46–52. [CrossRef]
42. Gens, A.; Alonso, E. A Framework for the Behaviour of Unsaturated Expansive Clays. *Can. Geotech. J.* **1992**, *29*, 1013–1032. [CrossRef]
43. Casini, F. Deformation Induced by Wetting: A Simple Model. *Can. Geotech. J.* **2012**, *49*, 954–960. [CrossRef]
44. Kim, Y.; Park, H.; Jeong, S. Settlement Behavior of Shallow Foundations in Unsaturated Soils under Rainfall. *Sustainability* **2017**, *9*, 1417. [CrossRef]
45. Liu, C.; Yan, Y.; Yang, H.-Q. Numerical Modeling of Small-Scale Unsaturated Soil Slope Subjected to Transient Rainfall. *Geosyst. Geoenviron.* **2023**, *2*, 100193. [CrossRef]
46. Francisca, F.M.; Giomi, I.; Rocca, R.J. Inverse Analysis of Shallow Foundation Settlements on Collapsible Loess: Understanding the Impact of Varied Soil Mechanical Properties during Wetting. *Comput. Geotech.* **2024**, *167*, 106090. [CrossRef]
47. COMSOL Multiphysics® 6.1; n.d. Available online: https://www.comsol.com/ (accessed on 15 August 2024).
48. Pedroso, D.M.; Farias, M.M. Extended Barcelona Basic Model for Unsaturated Soils under Cyclic Loadings. *Comput. Geotech.* **2011**, *38*, 731–740. [CrossRef]
49. Richards, L.A. Capillary Conduction of Liquids through Porous Mediums. *J. App. Phys.* **1931**, *1*, 318–333. [CrossRef]
50. Van Genuchten, M.T. A Closed-form Equation for Predicting the Hydraulic Conductivity of Unsaturated Soils. *Soil Sci. Soc. Am. J.* **1980**, *44*, 892–898. [CrossRef]
51. Mualem, Y. A New Model for Predicting the Hydraulic Conductivity of Unsaturated Porous Media. *Water Resour. Res.* **1976**, *12*, 513–522. [CrossRef]
52. Liang, C.; Cao, C.; Wu, S. Hydraulic-Mechanical Properties of Loess and Its Behavior When Subjected to Infiltration-Induced Wetting. *Bull. Eng. Geol. Environ.* **2018**, *77*, 385–397. [CrossRef]
53. Peranić, J.; Arbanas, Ž.; Cuomo, S.; Maček, M. Soil-Water Characteristic Curve of Residual Soil from a Flysch Rock Mass. *Geofluids* **2018**, *2018*, 6297819. [CrossRef]
54. Johari, A.; Talebi, A. Stochastic Analysis of Rainfall-Induced Slope Instability and Steady-State Seepage Flow Using Random Finite-Element Method. *Int. J. Geomech.* **2019**, *19*, 04019085. [CrossRef]
55. Johari, A.; Hooshmand Nejad, A. An Approach to Estimate Wetting Path of Soil–Water Retention Curve from Drying Path. *Iran. J. Sci. Technol. Trans. Civ. Eng.* **2018**, *42*, 85–89. [CrossRef]
56. Pham, H.Q.; Fredlund, D.G.; Barbour, S.L. A Study of Hysteresis Models for Soil-Water Characteristic Curves. *Can. Geotech. J.* **2005**, *42*, 1548–1568. [CrossRef]
57. Maswoswe, J. Stress Paths for Compacted Soil during Collapse Due to Wetting. Ph.D. Thesis, Imperial College, London, UK, 1985.
58. Seki, K.; Toride, N.; Van Genuchten, M.T. Evaluation of a General Model for Multimodal Unsaturated Soil Hydraulic Properties. *J. Hydrol. Hydromech.* **2023**, *71*, 22–34. [CrossRef]
59. Nian, G.; Chen, Z.; Bao, M.; Zhang, L.; Zhu, T. Rainfall Infiltration and Three-Dimensional Stability Analyses of Fractured Rock Slopes Considering Preferential Flow. *Nat. Hazards* **2023**, *118*, 2629–2656. [CrossRef]
60. Zhang, L.; Fredlund, D.; Zhang, L.; Tang, W. Numerical Study of Soil Conditions under Which Matric Suction Can Be Maintained. *Can. Geotech. J.* **2004**, *41*, 569–582. [CrossRef]
61. Alonso, E.; Romero, E. Collapse Behaviour of Sand; In Proceeding of the Asian conference on unsaturated soil, Osaka, Japan, 15–17 April 2003; pp. 325–334.